Sixth International Symposium on Turbulence and Shear Flow Phenomena
Seoul, Korea, 22-24 June 2009

TURBULENT EFFECTS OF LIQUID METAL FLOW UNDER STRONG FRINGING MAGNETIC FIELDS

X.Albets-Chico, D. Grigoriadis, S. Kassinos
Computational Science Laboratory – UCY-CompSci. Department of Mechanical and Manufacturing Engineering
University of Cyprus. 75 Kallipoleos, Nicosia 1678, Cyprus
e-mail: kassinos@ucy.ac.cy

B. Knaepen
Dynamics of Conductive Flows. Physique statistique et des plasmas (PSP). Université Libre de Bruxelles (ULB)
Campus de la Plaine. CP231, boulevard du Triomphe, 1050 Bruxelles, Belgium

ABSTRACT

This paper presents direct numerical simulations of a liquid metal flow under a space-varying magnetic field in an insulating circular duct. This is a generalization of a magnetohydrodynamic (MHD hereafter) benchmark case (MHD benchmark, 2005) in the nuclear fusion field. The benchmark was proposed after the experiments of Reed *et al.* (1987) owing to its similarity to the typical parameters appearing in liquid metal blankets of nuclear fusion reactors (Molokov and Reed, 2003). The main task at hand is to accurately define the transitional effects (suppression, triggering, intermittency) related to fringing magnetic fields and turbulence. For that purpose, the present paper addresses two qualitatively different cases: the first one considers the case of a turbulent flow ($Re_b = 7972$, $Re_\tau \approx 520$) entering a strong magnetic field (case MHD1) while the later considers the MHD flow leaving a strong magnetic field (case MHD 2). For brevity, this paper presents only some illustrative results concerning different Ha numbers for the case MHD1 and one very strong magnetic field ($Ha = 7000$) for the case MHD2. Additionally, preliminary purely hydrodynamic computations are presented (case HD, at an identical flow regime with the MHD cases). An excellent agreement has been obtained against both previous experimental (Durst *et al.*, 1995) and numerical results (Wagner *et al.*, 2001).

INTRODUCTION

MHD flows are of great interest in several industrial applications (liquid metal handling, glass processing, etc.) where the energetic demands are extremely large. On the other hand, fusion reactor devices (since the fusion blanket concept is based on self-cooled liquid metal which operates as a coolant and also as a breeder material) are intimately related to MHD flows. More concretely, liquid metal flows in circular ducts play a fundamental role in liquid metal blankets and divertors for fusion reactors. Concerning blankets, both inlet and outlet pipes have circular cross-section (Molokov and Reed, 2003). Due to the design of nuclear fusion reactors, liquid metal blankets are influenced by spatially varying magnetic fields. In such configurations, the action of the Lorentz force field produces complicated three-dimensional flow patterns. Under realistic conditions, turbulent effects are also expected to be present. Their comprehension and detailed analysis is of major importance as it could lead to very important improvements in terms of design optimization.

The MHD scientific community has historically applied simplified numerical approaches such as the asymptotic approximation (Molokov and Reed, 2003) to analyze these flow problems. However, only direct numerical simulations are able to study the related turbulent motions, as the asymptotic approach does not take into account inertia effects. The use of these simplified numerical techniques was unavoidable due to the extremely high computational demands related to wall-bounded MHD flows, especially for strong magnetic fields. Despite these numerical difficulties, in the present study a complete three-dimensional resolution of the discretized governing equations is adopted, using a finite volume approach.

FORMULATION

Governing equations

We consider a steady, three-dimensional flow of a viscous, electrically conducting, incompressible fluid in a straight, electrically insulating circular duct under the action of a spatially varying magnetic field $\mathbf{B} = B(x)\hat{\mathbf{y}}$ (Fig. 1). Under the conditions prevailing in fusion blankets, the magnetic Reynolds number ($R_m = \mu\sigma u_0 R$) is typically very small ($R_m << 1$) and the the induced magnetic field is negligible compared to the imposed magnetic field. In this case the isothermal flow is governed by the inductionless equations for the conservation of mass, momentum and charge:

$$\nabla \cdot \mathbf{u} = 0 \quad (1)$$

$$\frac{\partial \mathbf{u}}{\partial t} + \mathbf{u} \cdot \nabla \mathbf{u} = -\nabla p + \frac{1}{Re}\nabla^2 \mathbf{u} + N(\mathbf{j} \times \mathbf{B}) \quad (2)$$

$$\nabla \cdot \mathbf{j} = 0 \quad (3)$$

and by Ohm's Law

$$\mathbf{j} = \sigma(-\nabla\phi + \mathbf{u} \times \mathbf{B}) \quad (4)$$

$$\nabla^2 \phi = \nabla \cdot (\mathbf{u} \times \mathbf{B}), \quad (5)$$

where ν is the kinematic viscosity, σ is the electric conductivity and ρ is the fluid density. $\mathbf{u}$, $\mathbf{j}$, p, t and ϕ denote the dimensionless velocity, electric current density, pressure, time and electric potential, respectively. The characteristic scales for length, fluid velocity, time, electric current density, electric potential and pressure are R (the duct radius), u_0, R/u_0, $\sigma u_0 B_0$, $Ru_0 B_0$ and $R\sigma u_0 B_0^2$, respectively.

With the solenoidal current density field (eq. 3) and the Ohm's Law (eq. 4) one can derive a Poisson equation for

the electric potential (eq. 5) which is more convenient to treat numerically when compared to the Ohm's Law. In the equations above two dimensionless parameters appear: The Reynolds number $Re = u_0 R/\nu$ and the interaction parameter $N = R\sigma B^2/\rho\nu$. The former expresses the ratio between inertia and viscous forces, while the latter denotes the ratio between electrodynamic and inertia forces. From their combination a critical non-dimensional parameter can be derived: The *Hartmann* (Ha) number $Ha = RB\sqrt{\sigma/\rho\nu}$, which expresses the ratio between electrodynamic and viscous forces. Suppression of turbulence by the magnetic field in a round insulating pipe has been studied experimentally by many authors. Suppression of turbulence occurs for $Ha/Re > 0.025$ (Molokov and Reed, 2003). Moderate ($Ha \sim 50 - 2000$) and high magnetic fields ($Ha > 2000$) are present in nuclear reactor applications. According to previously reported studies, for the Reynolds number considered here ($Re_b = 7972$, $Re = 3986$), progressive decayment (case MHD1) and no turbulence (case MHD2) are expected in areas with high magnetic field intensity.

Boundary conditions

Boundary conditions at the wall, inlet, and outlet are required for the three variables in the governing equations, viz. the velocity components, pressure, and electric field. Due to the large space inhomogeneities created by the spatially varying magnetic fields, stream-wise periodic boundary conditions can not be applied and, therefore, inlet and outlet boundary conditions have to be specified.

Wall.

In this paper, the walls are considered to be impermeable to the fluid. So, a no-slip boundary condition, i.e. $\mathbf{u}|_{wall} = 0$ is used for the velocity field. The normal derivative of pressure at the walls is taken to be zero, i.e. $(\partial p/\partial n)|_{wall} = 0$. For the electric potential ϕ and non electrically conducting walls, a *Neumann* boundary condition $(\partial\phi/\partial n)|_{wall} = 0$ is applied, as the electrical fluxes at the walls are zero (see eq. 4).

Inlet.

The flow at the inlet is taken to have fully-developed conditions. To ensure an accurate velocity inlet profile is one of the most important parts of present work. As it can be inferred, the fully-developed conditions for the case MHD 1 (turbulent, purely hydrodynamic) are completely different from those for the case MHD 2 (magneto-hydrodynamic, laminar under strong magnetic fields). A brief explanation of the numerical techniques that have been applied to reproduce fully-developed conditions at the inlet will be exposed in next section.

Regarding the electric potential at the inlet, it is chosen to be compatible with the solenoidal current field (Mück *et al.* 2000), so that no electric current enters the computational domain, i.e. $(\partial\phi/\partial n)|_{inlet} = (\mathbf{u} \times \mathbf{B}) \cdot \mathbf{n}$. This is reduced in both MHD cases to $(\partial\phi/\partial n)|_{inlet} = 0$ (no magnetic field for the former, while $\mathbf{u} \parallel \mathbf{n}$ for the later due to the laminar flow conditions in such case).

Outlet

A convective boundary condition:

$$\frac{\partial \mathbf{u}}{\partial t} + U_{conv}\frac{\partial \mathbf{u}}{\partial n} = 0 \qquad (6)$$

is implemented at the outlet where $U_{conv} \equiv \frac{\int \mathbf{u} ds}{\int ds}$.

The boundary condition for the electric potential is also based on the same arguments applied at the inlet. Therefore, it is also chosen such that no electric current densities leave or enter the domain (Mück et al., 2000) which reduces to $(\partial\phi/\partial n)|_{outlet} = 0$, as well.

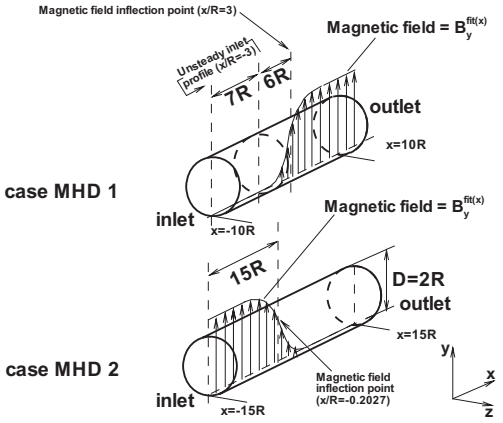

Figure 1: Qualitative description of the MHD cases.

The magnetic field

Both applied magnetic fields are based on *tanh* functions which fit the experimental data of the ALEX facility in the Argonne National Laboratory, (Picologlou *et al.*, 1986, Reed *et al.*, 1987). The present fitting function is derived from the one suggested in the MHD benchmark proposal (MHD Benchmark, 2005) for the decreasing magnetic field case.

For the case MHD 1, the increasing magnetic is defined as:

$$\text{MHD1} \rightarrow B_y^{\text{fit(x)}} = B_u \frac{1 + \tanh[0.45(x/R - 3)]}{2} \qquad (7)$$

The inflection point has been placed at $3R$ from the origin of coordinates (as indicated in Fig.1) in order to avoid the presence of the magnetic field in the hydrodynamic area, and thus ensuring that the purely turbulent inlet (extracted at $x/R = -3$, as further explained) will not be dampened by the magnetic field.

On the other hand, for the case MHD2, the decreasing magnetic field has been inspired by a slightly different *tanh*-fitting function in order to compare the present predictions with previous asymptotic results produced by Molokov and Reed (2003) when using a tanh-fitting with a decreasing factor of 0.8. Hence, the magnetic field has been chosen as:

$$\text{MHD2} \rightarrow B_y^{\text{fit(x)}} = \frac{1 - \tanh[0.8(x/R - 0.2027)]}{2} \qquad (8)$$

For more details, see (Albets-Chico, 2009) where a complete analysis of the decreasing magnetic field and a detailed comparison to Molokov and Reed (2003) results is carried out.

NUMERICAL ASPECTS

Numerical Techniques

A second-order accurate centered-difference scheme is used to discretize the diffusive and non-linear terms using finite volumes. The mass and momentum equations

	case MHD1	case MHD2
N_x	500	750
N_θ^{max}	225	156
N_r	∼62	∼45
$\Delta x/R$	0.04	0.04
$\Delta\theta_{max}/R$	0.028	0.0403
$\Delta r_{max}/R$	∼0.026	∼0.037
$\Delta r_{min}/R$	0.00005	0.00005

Table 1: Grid dimensionless sizes. The discretization in the radial direction is approximative (the core-grid is skewed and highly non-structured).

are coupled using a fractional-step method (Chorin, 1968) that avoids the *checkerboard* problem seen when standard interpolation methods are used for pressure. The electric potential values are obtained by solving the Poisson equation (5). Thus, at each computational time-step, two Poisson-type equations are solved, one for the pressure and one for the electric potential.

The equations (1) to (5) are solved in three dimensions using direct numerical simulations (DNS) on a nodal-colocated grid, i.e. $\mathbf{B}$, p, $\mathbf{j}$, and ϕ are computed at the cell center. The time integration of the flow equations is done using a Crank-Nicholson scheme for the diffusive terms. The non-linear terms are treated semi-implicitly and the Lorentz force is calculated explicitly. Therefore, the Lorentz force is the parameter that most significantly affects the numerical stability and mainly determines the time-step size, especially for high Ha numbers.

Grid-resolution requirements

In MHD flows, the boundary layers may become extremely thin at moderate and high Ha numbers due to the presence of electric current densities and Lorentz force effects near the wall. For example, the thickness of the *Hartmann* layer is inversely proportional to the Ha number, i.e. $\delta_{Ha} = O(Ha^{-1})$, and the dimensions of the *Roberts* regions fall inversely with the $-1/3^{\text{rd}}$ and $-2/3^{\text{rd}}$ power of the Ha number, i.e. $\delta_x \times \delta_y = O(Ha^{-1/3}) \times O(Ha^{-2/3})$ for the insulating circular duct illustrated in Figure 2. Therefore, the near-wall region must be resolved accurately in order to compute the shear stress not only in the viscous layers at high Reynolds numbers, but also in the *Hartmann* and *Roberts* layers, which might be thinner than the viscous layers at high Ha numbers.

Therefore, for the present study, the grid spacing is decreased closer to the wall to ensure that the sharp gradients in the *Hartmann* layers are calculated accurately up to $Ha \approx 10000$ as shown in Table 1. The mesh size at the core is chosen to be fine enough to capture all the turbulence details at hydrodynamic conditions. The wall-units sizes generated by the present meshes for HD conditions, at $Re_\tau \approx 520$, are for the case MHD1: $\Delta x^+ = 10.4$, $\Delta\theta^+_{max}$=7.2, $\Delta r^+_{max} \sim 7$, Δr^+_{min}=0.013; and for the case MHD2. $\Delta x^+ = 10.4$, $\Delta\theta^+_{max}$=10.4, $\Delta r^+_{max} \sim 10.2$, Δr^+_{min}=0.013.

The computation of the Lorentz force

At moderate ($\sim 50 - 2000$) and high (≥ 2000) Ha numbers, the accurate computation of the Lorentz force ($N(\mathbf{j}\times\mathbf{B})$) is the most challenging aspect in DNS calculations of MHD flows. As seen from Ohm's Law (equation (4)) the current density depends on $-\nabla\phi$ and $\mathbf{u}\times\mathbf{B}$. Indeed, such electrodynamic force (Lorentz force) is computed through a competition of these two terms ($-\nabla\phi$ and $\mathbf{u}\times\mathbf{B}$) that might be bigger than the other terms in equation (2) by several orders of magnitude (depending on the Ha number and the boundary conditions for the electric potential). Thus, small inaccuracies in estimating the Lorentz force terms can produce large errors in the momentum calculations resulting in highly inaccurate predictions of the flow behavior.

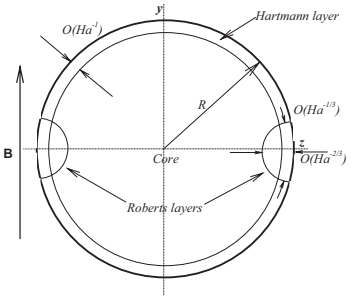

Figure 2: Cross section of a circular insulating duct and flow subregions at high Ha numbers. Figure extracted from Molokov and Reed (2003).

More concretely, the computation of the current densities is the most critical aspect. As pointed out by Ni *et al.* (2007), the resolution of equation (4) (when predicting the electrical potential gradient at the cell center by means of standard interpolation techniques) is only first-order accurate (and therefore charge is not conserved in the finite volume). When high electric potential gradients are present (for instance, high Ha numbers in insulating configurations, like the cases here addressed) this effect becomes critical and results are strongly distorted. Ni *et al.* (2007) proposed a different computation of the current density which relies on the idea to compute a conservative Lorentz force at the cell center when accurate information is available only at the cell faces. Thus, instead of solving equation (4) at the cell center, the current density is calculated by solving:

$$\mathbf{j} = \nabla \cdot (\mathbf{jr}) \tag{9}$$

The main advantage of this method is that the required information for computing the current density (and hence the Lorentz force) at the cell center is placed at the cell faces because $\mathbf{j}$ is computed from a volumetric divergence. Therefore, this scheme can apply the same order of numerical approximation used to resolve the electric potential without any additional interpolations, while conserving the charge in the finite volume at machine accuracy. A charge-conserving scheme has been applied in present work.

Numerical generation of the inlet boundary conditions

The generation of fully-developed conditions for the inlet is one of the key technical aspects of the present work. For the case MHD1, the unsteadiness of the fully-developed turbulence demands a time-depending inlet profile. For that, a plane has been sliced (at stream-wise position $x = -3R$, as depicted in Fig. 1) at each time-step (with given time=t_0). This plane has been injected at the inlet at each respective time=$t_0 + \Delta t$, while providing pseudo-periodic boundary-conditions for the sub-domain ($-10 \leq x/R \leq -3$ i.e. $7R$). The respective turbulent statistics (collected at $-10 \leq x/R \leq -3$) show a perfect agreement with present fully-developed turbulent stats obtained when using periodic boundary conditions as shown in Figures 3-4.

As to the case MHD2, the specification of inlet conditions becomes less complicated due to the laminar (and, therefore, two-dimensional and steady) flow generated by the strong

magnetic field applied at the inlet. For that purpose, a two-dimensional simulation with a constant magnetic field has been pre-computed and imposed later as a steady inlet profile.

RESULTS

Hydrodynamic results

The hydrodynamic simulation, based on the nuclear fusion benchmark case (Reed et *et al.*, 1987) was carried out first in order to test the numerical details that would yield satisfactory resolution of the turbulent motions.

Comparisons to both the experimental results from Durst *et al.* (1995) ($Re_b = 7442$) and the DNS from Wagner *et al.* (2001) ($Re_\tau = 500$) are presented in Figures 3-4. As shown, an excellent agreement is achieved and, consequently, the discretization details reveal themselves as acceptable parameters to analyze the turbulent effects for the Re_τ value considered. Additionally, results when applying pseudo-periodic inlet boundary conditions for the case MHD1 are also plotted to demonstrate the accuracy of the numerical strategy.

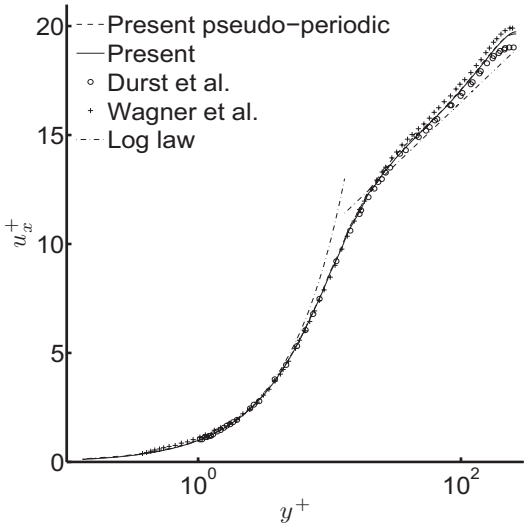

Figure 3: Axial mean velocity scaled on inner variables.

Magnetohydrodynamic results

The present paper analyzes the respective effects of different increasing magnetic fields (case MHD1 at $Ha = 50$, $Ha = 500$ and $Ha = 1000$) on fully-developed turbulent motion with perfectly electrically insulating walls. In the MHD2 case, a decreasing magnetic field under the effects of electrically insulating walls at Ha number of 7000 is presented. A high Ha number has been chosen in order to reproduce realistic conditions similar to those expected in the nuclear fusion blankets.

The task at hand is to determine quantitatively the suppression (for case MHD1) and the triggering of turbulence related to three-dimensional effects (for cases MHD1 and MHD2) for the liquid-metal flow under the specified conditions. For both cases, a potential difference along the stream-wise direction is established. This fact produces closed current density loops (see Figures 8 and 10) along the stream-wise direction which, in turn, generates Lorentz forces which are, depending on the area, perpendicular and parallel to the walls. The streamwise Lorentz forces generate braking and depending on the intensity of the magnetic field, may even create jets close to the walls and reverse flow in the core. In such a case the flow may become unstable or even turbulent even under the action of a strong magnetic field.

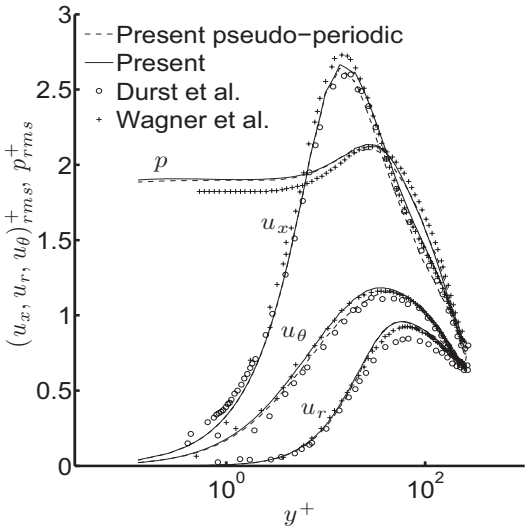

Figure 4: Root-mean-square (r.m.s.) velocities and pressure normalized by the wall friction velocity (u_τ) for both periodic and pseudo-periodic (inlet-outlet) boundary conditions applied in present work.

The present MHD computational parameters (i.e. appropriate resolution of Ha and side layers, electric balance) have been extensively tested when generating the inlet conditions for the case MHD2. The integrated mass fluxes and centerline velocities were found in agreement with the analytical solution with less than 2% of relative error for the higher Ha case considered here, viz. $Ha = 7000$.

Case MHD1.

A parametric study has been carried out in order to assess how changes in the intensity of the magnetic field act upon the turbulent motions. The first case ($Ha^R = 50, Re_b^R = 3986$; i.e. $Ha/Re = 0.0125$) does not lead to a complete turbulence suppression. It is important to note that no advective additional effects (such as jets) appear, as the intensity of the Lorentz forces is not sufficient to generate important by-passes in the flow. Hence, the remaining turbulent fluctuations are only generated by the upstream turbulent field. Fig. 5 presents the power spectra and the time history of streamwise velocity at the centerline position (viz. $y/R = 0$, $z/R = 0$) for upstream ($x/R = -5$) and downstream ($x/R = 9$) locations. As shown, the turbulent fluctuations are damped but not completely eliminated. This agrees with Molokov and Reed's (2003) claim that the suppression of turbulence occurs for $Ha/Re > 0.025$.

According to the last statement, a complete suppression of turbulence should occur at $Ha = 500$ and $Ha = 1000$ cases. Nevertheless, as important shear effects are related to the stream-wise voltage difference, turbulence persists under the combined action of the damping effects of the cross-stream-wise Lorentz forces (viz. $[\mathbf{j} \times \mathbf{B}]|_{y,z}$) and the strong shear generated by the braking stream-wise Lorentz force (viz. $[\mathbf{j} \times \mathbf{B}]|_x$).

Fig. 6 presents the power spectra and the time-history of the streamwise velocity component for the $Ha = 1000$ case at the centerline ($y = 0$, $z = 0$) for both upstream

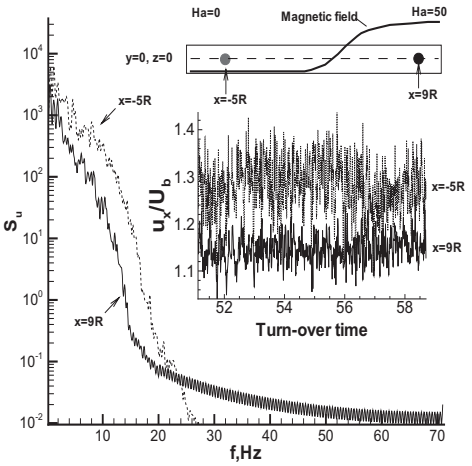

Figure 5: Case MHD1. $Ha = 50$. Time-history of the streamwise velocity component and related power spectra at the centerline.

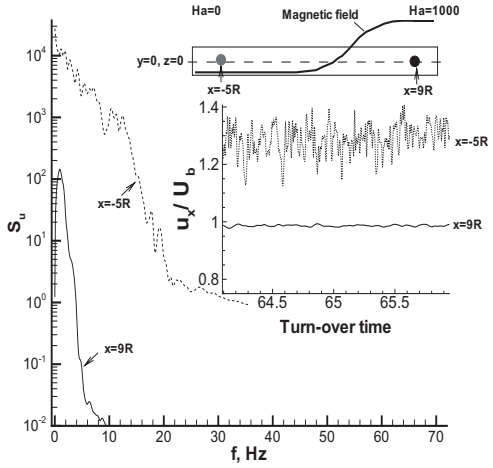

Figure 6: Case MHD1. $Ha = 1000$. Time-history of the streamwise velocity component and related power spectra at the centerline.

(HD probe) and downstream locations (MHD probe). As it can be seen, although the turbulent fluctuations are clearly attenuated downstream, they are not completely damped despite the fact that the non-dimensional parameter Ha/Re is almost ten times higher than the theoretical limiting value.

At the vicinity of the wall ($y = 0$, $z = 0.95R$), more energetic power spectra were obtained and less attenuation downstream took place with respect to the centerline, as depicted in Fig. 7. This effect occurs because of the combined action of the boundary layer instability and the shear effects generated by the jets.

Furthermore, as shown in Fig. 8c, the intensity of the streamwise velocity fluctuations is almost two times higher than the hydrodynamic values in the areas where the jets are generated at $x/R \approx 6$. It is important to note that although these jets fluctuate strongly, they are not essentially turbulent since spectral analysis has revealed that these fluctuations contain only two frequencies. This effect can also be seen in Fig. 9, where non-turbulent instabilities are present at $x/R = 6$ and at $x/R = 9$ positions.

This effect is also apparent for the $Ha = 500$ case in Fig. 8b, where moderate jets have already appeared and the

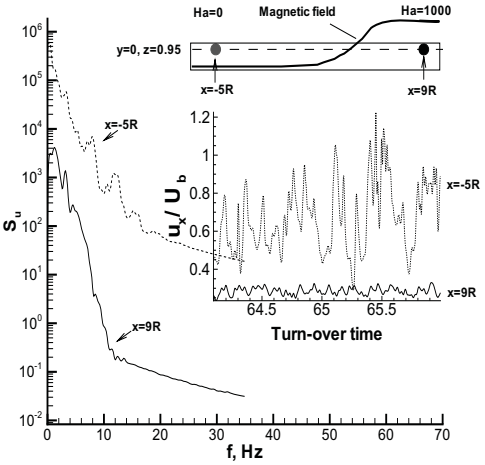

Figure 7: Case MHD1. $Ha = 1000$. Time-history of the streamwise velocity component and related power spectra close to the wall.

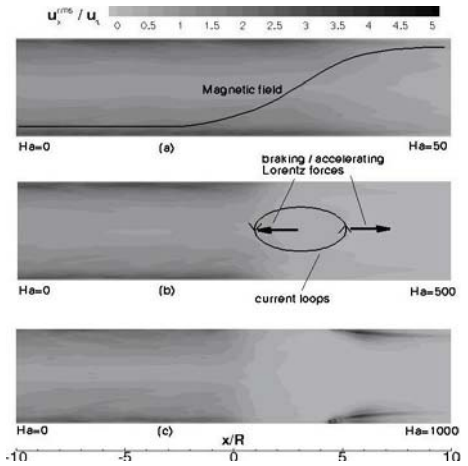

Figure 8: Case MHD1. u_x^{rms}/u_τ for $Ha = 50$ (a), $Ha = 500$ (b) and $Ha = 1000$ (c).

turbulent fluctuations are promoted by the convective jets. The persistence of turbulence in such strong magnetic fields is partially explained by the by-pass effect produced by the braking Lorentz force as schematically depicted in Fig. 8b. It is important to note that this effect was not present for the lower Ha number considered where turbulence intensities were smoothly damped by the action of the magnetic field (Fig. 8a).

Case MHD2.

As in the previous case MHD1, preliminary computations carried out for the case MHD2, have shown that the shape and intensity of the jets depend on the established voltage difference and, therefore, on the Ha number. For instance, at $Ha = 1000$ jets with a maximum speed around 3.5 times the bulk velocity appear. In this case, the related turbulent structures tend to relaminarize as the intensity of the jets appears not to be sufficiently strong to sustain turbulence. Paradoxically, the bigger the Ha number, the bigger the damping of the turbulence in the high magnetic field area, but also the higher the voltage difference and, hence, the more important the three-dimensional turbulent effects in the magnetic-free field area.

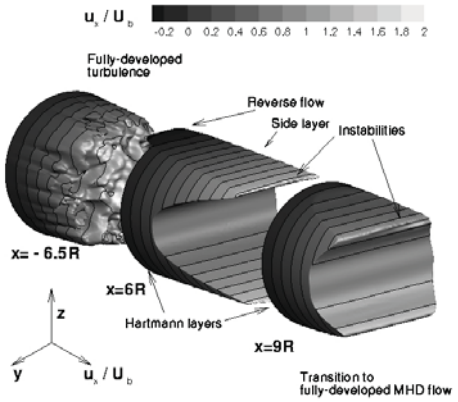

Figure 9: Case MHD1. $Ha = 1000$. Instantaneous velocity field for three different stream-wise positions.

Fig. 10 presents a snapshot of the dimensionless pressure, instantaneous stream-wise velocity and stream-wise velocity fluctuations (r.m.s.). As shown, most of the pressure drop is localized in the high-magnetic field area (where a completely laminar flow is present) due to the sharp *Hartmann* layers which produce higher shear at the walls. While the magnetic field decreases, the current-densities loops generate a strong braking Lorentz force in the core. Jets (around 18 times the bulk velocity) take place close to the walls ($z = \pm R$, where the currents are parallel to the walls and the braking Lorentz force vanishes). Further downstream, in the absence of magnetic field, strong turbulent motions are present. They are clearly linked with such three-dimensional effects. It is important to note that the fluctuations computed for this case are one order of magnitude larger than the typical hydrodynamic ones for the same Re_b, when using the hydrodynamic friction velocity (u_τ) to rescale the statistics.

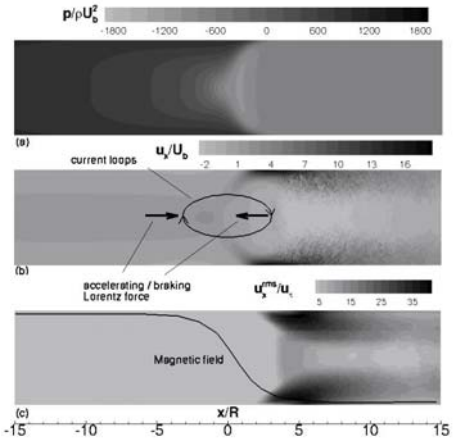

Figure 10: Case MHD2. $Ha = 7000$. Dimensionless pressure (a), stream-wise velocity (b) and u_x^{rms} (c).

CONCLUDING REMARKS

The flow patterns generated in a liquid metal flow under spatially-varying magnetic fields in an insulating pipe are strongly influenced by the intensity of the magnetic field. Experimental studies have shown that turbulence tends to be completely suppressed when $Ha/Re > 0.025$. Nevertheless, under fringing magnetic fields, three-dimensional effects related to the braking Lorentz forces may produce jets and even reverse flow for very strong magnetic fields. Non-linear effects are, hence, generated and turbulent effects may appear.

Under increasing magnetic fields, turbulence is progressively damped in the stream-wise direction. The present study shows, however, that local peak intensities of the fluctuations due to the three-dimensional effects may appear even under strong magnetic fields. Further research needs to be done in order to state if this phenomena might enhance turbulence.

Under decreasing magnetic fields, if the three-dimensional effects are sufficiently strong, the triggering of turbulence is very rapid. The intensity of the turbulent fluctuations may become higher than typical HD turbulence by one order of magnitude for $Ha = 7000$.

REFERENCES

Albets-Chico, X., Knaepen, B., Radhakrishnan, H. & Kassinos, S. (2009)"Numerical analysis of liquid metal flow under a fringing magnetic field", *to be submitted*.

Chorin A. J. (1968). "Numerical Solution of the Navier-Stokes Equations", *Mathematics of Computation*. Vol. 22, No.104, pp 745-762.

Durst F., Jovanoviĉ J., Sender J. (1995). "LDA measurements in the near-wall region of a turbulent pipe flow". *J. Fluid Mech.*. Vol. 295, pp. 305-335.

MHD benchmark. 2005. "Liquid Metal Flow Leaving a Strong Magnetic Field". Tech. Rep. *IEA Liquid Breeder Blanket SubTask on MHD* (june 3, 2005)

Molokov, S. and Reed, C. B. (2003). "Parametric study of the liquid metal flow in a straight insulated circular duct in a strong nonuniform magnetic field". *Fusion Science and Technology*, Vol. 43, pp. 200-216.

Mück, B., Günther C., Müller U., Bühler L. (2000). "Three-dimensional MHD flows in rectangular ducts with internal obstacles".*Journal of Fluid Mechanics*. Vol 418, pp. 265-295.

Picologlou B.F., Reed C., Dauzvardis P. (1986). "Experimental and analytical investigations of Magnetohydrodynamic flows near the entrance to a strong magnetic field", *Fusion Technology*. Vol. 10, pp. 860-863

Reed, C. B., Picologlou B.F., Hua T.Q. (1987). "ALEX results - A comparison of measurements from a round and rectangular duct with 3-D code predictions".*In Proc. IEEE 12th Symposium on Fusion Engineering*, Monterey, California, October 13-16. pp.1267-1270.

Wagner C., Hüttl T.J., Friedrich R. (2001). "Low-Reynolds-number effects derived from direct numerical simulations of turbulent pipe flow". In *Computers and fluids*, Vol. 30, pp. 581-590.

ACKNOWLEDGEMENTS

The authors are thankful to Prof. Leo Bühler, whose suggestions partially motivated the present study. This work has been performed under the UCY-CompSci project, a Marie Curie Transfer of Knowledge (TOK-DEV) grant (Contract No. MTKD-CT-2004-014199). This work has also been partially performed under the EURYI (European Young Investigator) Awards scheme and under a Center of Excellence grant from the Norwegian Research Council to the Center of Biomedical Computing. Finally, the first author would also like to thank the friends at the art-culture residence "Cal Gras" (Avinyó, Barcelona) where the first lines of present code were written during Christmas 2008.